Influence of Förster interaction on light emission statistics in hybrid systems

T. Sverre Theuerholz,[1,*] Alexander Carmele,[1,2] Marten Richter,[1] and Andreas Knorr[1]

[1]*Institut für Theoretische Physik, Nichtlineare Optik und Quantenelektronik, Technische Universität Berlin, Hardenbergstr. 36, 10623 Berlin, Germany*

[2]*Institut für Quantenoptik und Quanteninformation, Technikerstr. 21a 6020 Innsbruck, Austria*

(Received 10 April 2013; revised manuscript received 22 May 2013; published 24 June 2013)

We investigate the influence of the Förster interaction between semiconductor quantum dots on the quantum light emission in proximity to a metal nanoparticle. A fully quantized theory for the excitons in the quantum dots, the plasmons in metal nanoparticles, and their interaction is used. Using an operator equation approach, we derive the Rayleigh emission spectra and the corresponding quantum statistics of the emission. For both observables, we investigate the influence of the exciton-plasmon coupling and the Förster interaction between the semiconductor quantum dots. Surprisingly, the influence of the Förster interaction is barely seen in the Rayleigh spectra whereas the second-order correlation function is strongly affected. In particular, we show that the Förster interaction is capable to tune the emission statistics: depending on the system parameters, the Förster interaction between the semiconductor quantum dots induces strong bunching and antibunching of the emission, respectively. We analyze the quasiparticles formed in the coupled system to explain the observed features.

DOI: 10.1103/PhysRevB.87.245313 PACS number(s): 73.40.Vz, 78.67.Bf, 78.67.Hc, 78.20.Bh

I. INTRODUCTION

Recently, hybrid structures, consisting of a metal nanoparticle (MNP) and semiconductor quantum dots (SQD), are intensively studied, theoretically and experimentally. Such devices combine the advantages of both materials for new applications, such as ultrasensitive,[1] biosensing[2], and light-harvesting devices,[3] devices for quantum information,[4] and nanoscale laser cavities (spaser).[5,6]

MNPs are usually made of noble metals because of their low resistance. Here, the electrons in the conduction band of the MNP are able to build up collective plasmonic oscillations. In contrast, for optical excitations of SQDs, a conduction-band electron and a valence-band hole form an exciton. As long as no direct charge transfer between both particles is possible, the interaction between the SQDs and the MNP is mediated by the Coulomb interactions, such as Förster transfer, between plasmons and excitons. This interaction causes several effects that can be explained within a semiclassical theory of light matter interaction: due to the energy transfer between the SQD and the MNP, characterized by a strong damping of the plasmon excitation, the SQD excitonic lifetime decreases.[7] The interference of the external and internal fields has a strong impact on the absorption and Rayleigh spectra.[8] Furthermore, the interaction shifts the excitonic transition energy[9] and Rabi oscillations may occur in case of strong electron-light coupling.[10] Quantum optical experiments allow also to investigate the statistics of emitted light: previously Ridolfo *et al.*[8] have investigated theoretically the photon/plasmon statistics of one SQD and one MNP. They showed a strong impact of the interaction between the SQD and the MNP on the statistics of the light emitted by the interacting hybrid system. In our work, we extend the previously investigated hybrid structure and include the Förster interaction between two different SQDs coupled to one MNP. Investigating the linear Rayleigh spectra, we found that the influence of the Förster interaction between different SQDs is barely seen. In strong contrast to this, the statistics of the emitted field is dramatically changed, since it is determined by nonlinear properties. In particular, we show that it is possible to tune the second-order correlation function of the light emission by the Förster interaction between the quantum dots. Figure 1 shows a sketch of the hybrid system we study in this paper. The paper is organized as follows. First, we develop a theoretical description of the MNP-two SQDs hybrid system and characterize the spectral emission via the linear Rayleigh spectrum. Afterwards, we focus on the second-order correlation function of the emission and investigate the influence of the SQD-Förster interaction on the emission statistics.

II. THEORETICAL MODEL

We describe the MNP and the SQDs as well as their interaction within the dipole approximation. This is valid as long as the radii of the SQD and the MNP are small compared to the distance between them.[11] Van Vlack *et al.* showed, by using a Green function formalism, that multipole effects are negligible if the distance between the SQDs and the MNP is at least the diameter of the MNP.[12] In this case, the dipole approximation and a more precise theory including multipole effects yield the same results. Furthermore, the size of the MNP and the SQDs need to be much smaller than the wavelength of the incident light, in this case, a quasistatic approach is valid.[6] The full Hamiltonian reads $H = H_0 + H_{\text{int}} + H_{\text{ext}} + H_F$. H_0 contains the contributions of the noninteracting hybrid system:

$$H_0 = H_{\text{pl}} + H_{\text{exc}} = \hbar\omega_{\text{sp}} a^\dagger a + \hbar \sum_i \omega_{g_i} a_{c_i}^\dagger a_{c_i}, \qquad (1)$$

with the surface plasmon resonance frequency ω_{sp} and the transition energy $\hbar\omega_{g_i}$ of the ith SQD. $a_{c_i}^\dagger$ and a_{c_i} are the creation and annihilation operators for an electron in the conduction band of the ith SQD—these operators satisfy Fermi commutation relations. We set the energy of the valence band to zero. $a^\dagger$ and a are the bosonic creation and annihilation operators for the plasmons.

The Hamilton operator for the dipole-dipole interaction between the MNP and the SQDs in the rotating wave

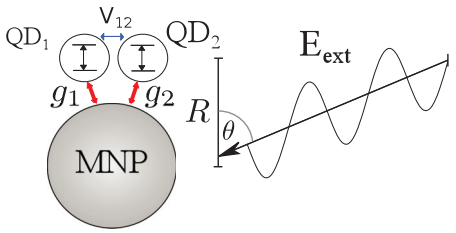

FIG. 1. (Color online) Sketch of the hybrid system: two interacting (V_{12}) SQDs (QD_1, QD_2) are coupled to a spherical MNP (g_1, g_2). We assume that the SQDs are close to each other and therefore have the same angle and distance with respect to the spherical MNP.

approximation (RWA) is given by[8]

$$H_{\text{int}} = -\hbar \sum_i g_i a_{v_i}^\dagger a_{c_i} a^\dagger + \text{H.c.}, \tag{2}$$

where g_i denotes the coupling strength between the ith SQD and the MNP. The system is excited by an external optical field. Applying the RWA simplifies the interaction Hamiltonian of the hybrid system with the external field to

$$H_{\text{ext}} = -E_t \chi a^\dagger - \sum_i \mu_i E_t a_{c_i}^\dagger a_{v_i} - \text{H.c.} \tag{3}$$

The external optical field $E_t = E_0 e^{-\mathbb{i}\omega_{\text{ext}} t}$ consists of the amplitude E_0 and is oscillating with ω_{ext}. We define the laser amplitude $E_0 = \frac{\Omega}{2\mu_i}$ through the Rabi energy Ω and the dipole moment of the ith SQD μ_i.

Furthermore, we include the dipole-dipole-interaction between different SQDs, in the form of the Förster interaction:[13,14]

$$H_F = \sum_{\substack{i,j \\ i \neq j}} \left(V_{ij} a_{c_i}^\dagger a_{v_j}^\dagger a_{c_j} a_{v_i} + \text{H.c.} \right). \tag{4}$$

The Förster interaction describes dipole-dipole excitation transfer from the jth SQD to the ith SQD (the complex conjugated term describes the opposite transfer). This interaction plays an important role in, e.g., the excitation transfer on nanoscales[14] and in the stabilization of self-induced coherence.[15]

In addition to the coupling to the external field and the Förster-coupling of MNP and SQDs, internal interactions in the single SQD and MNP constituents account for dissipative effects. Typical examples include electron-phonon coupling, which introduces damping of the individual plasmons and excitons. Damping is included via Lindblad contributions $\mathfrak{L}$.[16] These terms describe the interaction of the plasmons and excitons with a reservoir (phonons, other electron reservoirs etc.):

$$\begin{aligned} \mathfrak{L}_{\text{sp}} &= \frac{\gamma_{\text{sp}}}{2}(2a\rho a^\dagger - a^\dagger a\rho - \rho a^\dagger a) \text{ for the plasmons and} \\ \mathfrak{L}_g &= \frac{\gamma_g}{2}\left(2\rho_{vc_i}\rho\rho_{vc_i}^* - \rho_{vc_i}^*\rho_{vc_i}\rho - \rho\rho_{vc_i}^*\rho_{vc_i}\right) \\ &\quad \text{for the } i\text{th SQD } \left(\rho_{vc_i} = a_{v_i}^\dagger a_{c_i}\right), \end{aligned} \tag{5}$$

where γ_{sp} is the damping rate of the plasmons and γ_g determines the decay of the exciton, describing, e.g., energy relaxation of the system due to losses. For example, Ohmic losses in the metal account for the plasmon damping and radiative decay channels account for the exciton damping.

The quantum-mechanical dynamics of the density matrix is calculated using the operator equation[16]

$$\frac{d}{dt}\rho = \frac{\mathbb{i}}{\hbar}[\rho, H] + \mathfrak{L}_{\text{sp}} + \mathfrak{L}_g. \tag{6}$$

Typical observables, e.g., the plasmon density $\langle a^\dagger a \rangle$, are calculated by tracing over the density operator $\langle a^\dagger a \rangle = \text{tr}(a^\dagger a \rho)$. Before we discuss this in detail, we estimate the coupling constants χ of the MNP to the external field and the coupling strength g_i between the MNP and the ith SQD. We follow Refs. 8 and 17 and use the equation of motion for the coherent plasmon mode excitation and formally solve it in Fourier space:

$$\langle a \rangle(\omega) = \frac{\mathbb{i} g}{D(\omega)} \langle a_{v_i}^\dagger a_{c_i} \rangle(\omega) + \frac{\mathbb{i}\chi}{\hbar D(\omega)} E_0, \tag{7}$$

where $D(\omega) = \mathbb{i}(\omega_{\text{sp}} - \omega) + \gamma_{\text{sp}}/2$. Comparing the expressions for the classical field and the quantum-mechanical dipole field, yields for the coupling parameter between MNP and SQDs:

$$g_i = \mathbb{i} \frac{s_\alpha}{\hbar R^3} \sqrt{\frac{3\hbar\eta r_m^3}{4\pi\varepsilon_0}}, \tag{8}$$

and for the external field-plasmon coupling,

$$\chi = -\varepsilon_b \sqrt{12\pi\hbar\eta\varepsilon_0 r_m^3}. \tag{9}$$

For a detailed calculation of g_i and χ, see the calculation in Refs. 8 and 17. Here, r_m is the radius of the MNP, ϵ_b the permittivity of the surrounding medium, and $s_\alpha = 3\cos^2(\theta) - 1$. The angle θ lies between the axis of the hybrid system and the external optical field cf. Fig. 1. $\eta = \{\frac{d(\text{Re}[\epsilon_{\text{MNP}}(\omega)])}{d\omega}|_{\omega=\omega_{\text{sp}}}\}^{-1}$ is the inverse of the gradient of the real part of the dielectric function of the metal at the plasma frequency.

For all calculations in the following sections, we use dipole moments $\mu_i = 0.52\, e$ nm for the SQDs and a Förster interaction strength of at most $V_{12} = 0.45$ meV possible for CdSe SQDs,[18,19] with a damping of the excitons of $\gamma_g = 1$ meV. We assume $\varepsilon_b = 3$ for the media surrounding the hybrid system. We choose a silver MNP with radius $r_m = 5$ nm, this yields $\chi = 14.45\, e$ nm, the plasmon damping is $\gamma_{\text{sp}} = 53.31$ meV, and the plasma frequency is $\hbar w_{\text{pl}} = 2.89$ eV.[20]

III. OBSERVABLES

In this section, we introduce the observables of interest. We focus on the macroscopic polarization $P_{\text{mac}}(\omega)$ to discuss Rayleigh spectra and the second-order correlation function $g^{(2)}$ to characterize the emission statistics. The macroscopic polarization is given by the sum of the microscopic polarization P_{mic} of the whole system:

$$P_{\text{mac}} = P_{\text{mic}}^\dagger + P_{\text{mic}} = \chi a^\dagger + \sum_i \mu_i a_{c_i}^\dagger a_{v_i} + \text{H.c.} \tag{10}$$

Using the source field expression for the emitted field,[21] the intensity of the Rayleigh scattering signal I_S in frequency domain is given by

$$I_S(\omega) = \langle P_{\text{mac}}^\dagger P_{\text{mac}} \rangle(\omega) \approx |\langle P_{\text{mac}}(\omega) \rangle|^2, \tag{11}$$

the factorization is valid if the densities are negligible, e.g., in the weak-field limit of linear optics.[16]

For realistic values of the hybrid system parameters, it has been shown that the far-field is mainly determined by the plasma oscillations in the metal.[22] Therefore the Rayleigh scattering signal is basically given by $P_{\mathrm{mic}} = \chi a^\dagger$, i.e., $I_S(\omega) = \chi^2\langle a^\dagger a\rangle(\omega) \approx \chi^2|\langle a\rangle(\omega)|^2$, we will motivate this approximation in more detail in Sec. V. Similarly, the statistics of the light emission in the far field is dominated by the second-order correlation function of the plasmons, defined via the ratio of the plasmon density correlation $\langle a^\dagger a^\dagger aa\rangle$ and the square of the plasmon density $\langle a^\dagger a\rangle$:

$$g^{(2)}(t) = \frac{\langle a^\dagger a^\dagger aa\rangle(t)}{\langle a^\dagger a\rangle(t)^2}. \tag{12}$$

IV. EQUATION OF MOTION

We derive the equation of motion for the observables, Eqs. (11) and (12), using the operator equation (6). Before we do this, we note that within the many-body hierarchy, typical quantities, for example, the plasmon density $\langle a^\dagger a\rangle$ couples to plasmon transition $\langle a^\dagger\rangle$ and the SQD assisted polarizations $\langle a^\dagger_{v_i} a_{c_i} a^\dagger\rangle$:

$$\frac{d}{dt}\langle a^\dagger a\rangle = -\gamma_{\mathrm{sp}}\langle a^\dagger a\rangle - 2\sum_i \mathrm{Im}\left(g_i\langle a^\dagger_{v_i} a_{c_i} a^\dagger\rangle\right) - \frac{2}{\hbar}\chi\,\mathrm{Im}(E_t\langle a^\dagger\rangle). \tag{13}$$

Also, the equation of motion of the source term $\langle a^\dagger_{v_i} a_{c_i} a^\dagger\rangle$ couples to even higher orders of plasmonic operators. In order to circumvent the hierarchy problem for the observables, we introduce number states for the bosonic plasmons. For systems with only a few SQDs, this formalism yields more precise results than factorization schemes like, e.g., the cluster expansion, which is valid if several SQDs are involved.[23] The number states enable us to evaluate the equation of motion numerically up to the crucial order n in the plasmon number states. Here, the number states represent the eigenstates $|n\rangle$ of the plasmonic system, $H_{\mathrm{pl}}|n\rangle = \hbar\omega_{\mathrm{sp}} n|n\rangle$. All plasmonic and excitonic expectation values can be expressed through number states. Also, we find that this method is more robust compared to a standard correlation expansion.[23] As an example, we express the polarization and the $g^{(2)}$ through number states:

$$\begin{aligned}\langle P_{\mathrm{mac}}\rangle &= \chi\sum_{n=0}^{\infty}\langle a^\dagger|n\rangle\langle n|\rangle + \mathrm{H.c.}\\ &= \chi\sum_{n=0}^{\infty}\sqrt{n+1}\langle|n+1\rangle\langle n|\rangle + \mathrm{H.c.}\end{aligned} \tag{14}$$

$$g^{(2)}(t) = \frac{\sum_{n=0}^{\infty}\langle a^\dagger a^\dagger aa|n\rangle\langle n|\rangle}{\left(\sum_{n=0}^{\infty}\langle a^\dagger a|n\rangle\langle n|\rangle\right)^2} = \frac{\sum_{n=0}^{\infty} n(n-1)\langle|n\rangle\langle n|\rangle}{\left(\sum_{n=0}^{\infty} n\langle|n\rangle\langle n|\rangle\right)^2}.$$

From Eq. (14), it can be recognized that one needs diagonal, nondiagonal, and operator $\hat{O} = \hat{O}(a^\dagger, a)$ assisted expectation values of $|n\rangle\langle m|$ to describe the dynamics. To include also the off-diagonal elements $\langle\hat{O}|n\rangle\langle m|\rangle$ $(n \neq m)$ up to the crucial order, we start with the general derivation of $p_{n,m} = \langle|n\rangle\langle m|\rangle$. Using the conservation of charges for the conduction n_c and valence n_v band $(n_c + n_v = 1)$, $p_{n,m}$ can be expressed in the biexciton base:

$$p_{n,m} = n^{n,m}_{v_1} + n^{n,m}_{c_1} = \langle\rho^{n,m}_{vvvv}\rangle + \langle\rho^{n,m}_{vccv}\rangle + \langle\rho^{n,m}_{cvvc}\rangle + \langle\rho^{n,m}_{cccc}\rangle. \tag{15}$$

This quantity describes the probability of finding n plasmons (if $n = m$) and the transition probability of m to n plasmons (if $n \neq m$), respectively. Here, contributions of the form $\rho^{n,m}_{opqr}$ are defined for $o,p,q,r \in c,v$ (c: conduction, v: valence band) as: $\rho^{n,m}_{opqr} = a^\dagger_{o_i} a^\dagger_{p_j} a_{q_j} a_{r_i}|n\rangle\langle m|$, corresponding to the operators of the ith and jth SQDs, respectively.

Restricting ourselves to two SQDs, the equation of motion for $\langle\rho^{n,p}_{cccc}\rangle$ reads

$$\begin{aligned}\partial_t\langle\rho^{n,m}_{cccc}\rangle = &\left[\mathbb{i}(n-m)\omega_{\mathrm{sp}} - \frac{\gamma_{\mathrm{sp}}}{2}(n+m) - 2\gamma_g\right]\langle\rho^{n,m}_{cccc}\rangle + \gamma_{\mathrm{sp}}\sqrt{n+1}\sqrt{m+1}\langle\rho^{n+1,m+1}_{cccc}\rangle\\ &- \mathbb{i}\sqrt{n+1}\left(g_1\langle\rho^{m,n+1}_{cccv}\rangle^* + g_2\langle\rho^{m,n+1}_{ccvc}\rangle^*\right) + \mathbb{i}\sqrt{m+1}\left(g_1^*\langle\rho^{n,m+1}_{cccv}\rangle + g_2^*\langle\rho^{n,m+1}_{ccvc}\rangle\right)\\ &- \mathbb{i}\frac{\mu_1}{\hbar}\left(E_t^*\langle\rho^{m,n}_{cccv}\rangle^* - E_t\langle\rho^{n,m}_{cccv}\rangle\right) - \mathbb{i}\frac{\mu_2}{\hbar}\left(E_t^*\langle\rho^{m,n}_{ccvc}\rangle^* - E_t\langle\rho^{n,m}_{ccvc}\rangle\right)\\ &+ \frac{\mathbb{i}}{\hbar}E_t^*\chi^*\left(\sqrt{m+1}\langle\rho^{n,m+1}_{cccc}\rangle - \sqrt{n}\langle\rho^{n-1,m}_{cccc}\rangle\right) + \frac{\mathbb{i}}{\hbar}E_t\chi\left(\sqrt{m}\langle\rho^{n,m-1}_{cccc}\rangle - \sqrt{n+1}\langle\rho^{n+1,m}_{cccc}\rangle\right).\end{aligned} \tag{16}$$

The first line originates from the free rotation and the Lindblad contributions, describing the damping and inscattering from higher transition probabilities. The second line describes the interaction between the excitons and plasmons. The last two lines arise from the interaction with the external field E_t. Via coupling to higher plasmon orders, the hierarchy problem is rediscovered. However, we know from previous investigations,[23] that the number state hierarchy is more easy to treat compared to an operator hierarchy as in Eq. (13), since we get a closed form for all orders.

The whole coupling scheme of dynamical quantities fulfilling a self-consistent hierarchy of dynamical equations is depicted in Fig. 2 and the equation of motions can be found in Appendix B. Considering two SQDs with one electron per SQD, the hierarchy is closed at the level of expectation values with four fermionic operators. Numerically, we evaluate the equations of motion up to the crucial order (u) in the plasmon transitions. At this order, $\rho^{u+1,u+1}_{opqr} \approx 0$ holds. For weak external excitation $\Omega = 10^{-6}$ eV, the relevant order is $u = 4$. For the initial conditions, we assume the SQD electrons

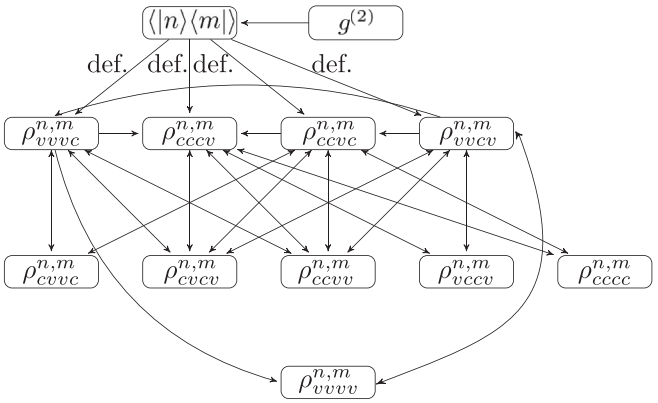

FIG. 2. Coupling diagram for the equations of motion starting from the second-order correlation function as a relevant observable. Involved quantities are the generalized transition probability $p_{n,m}$ and plasmon transition assisted by four fermionic operators $\rho^{n,m}_{opqr}$.

in the ground state and a Bose-Einstein distribution ($T = 300$ K) for the plasmon probability $p_{n,n}$, all other correlations, in particular, $p_{n,m}(n \neq m)$ equal zero. Furthermore, factoring initial conditions for the individual systems are assumed.

V. OPTICAL EMISSION SPECTRA: CHARACTERIZATION OF THE SYSTEM

First, to characterize the SQD-plasmon hybrid system, we study the linear Rayleigh spectrum. For this, we use a δ pulse excitation $\Omega(t) = E_0\delta(t)$ in time domain for the external light pulse and calculate the macroscopic polarization $P(t)$, Eq. (10), in time domain. Afterwards, we performed a Fourier transformation to obtain the linear Rayleigh spectra. All parameters used can be found in the caption of Fig. 3, we use parameters for CdSe SQDs.[18,19]

In Fig. 3(a), we plot the Rayleigh spectrum of a bare MNP and two resonant SQDs without plasmon-SQD coupling. The far-field spectrum of the bare MNP is spectrally broadened due to the large damping γ_{sp} of the plasmons induced by ohmic losses in the metal. As a consequence of the long lifetime (radiative, pure dephasing such as interaction with phonons) of the exciton, in comparison to the MNP, the two bare SQDs exhibit a narrow peak. The Förster interaction slightly shifts the transition energies of the coupled SQDs [Fig. 3(a), $V_{12} = 0.45$ meV]. Figures 3(b), 3(c), 3(e), and 3(f) display the spectrum of the coupled MNP-SQD hybrid system for $R = 10$ nm (corresponding to $g = 10.96$ meV) and $R = 13$ nm (corresponding to $g = 4.99$ meV), respectively. For Figs. 3(b) and 3(e), the SQDs and MNP are assumed to be in resonance. Due to the interaction, new states with slightly modified transition energies are formed, recognizable by the two peaks of the linear Rayleigh spectrum. The newly formed states are a superposition of the uncoupled states of the bare SQDs and the bare MNP (cf. Appendix A). These spectra are similar to the spectra calculated in Ref. 8. The vanishing spectral contribution at $\Delta = 0$ meV is caused by a destructive interference of the real and imaginary parts of P_{mac} originating from the two peaks originating from the hybridization.

We include the coherent Förster interaction between the SQDs [dashed green lines in Figs. 3(b)–3(f)] in addition to

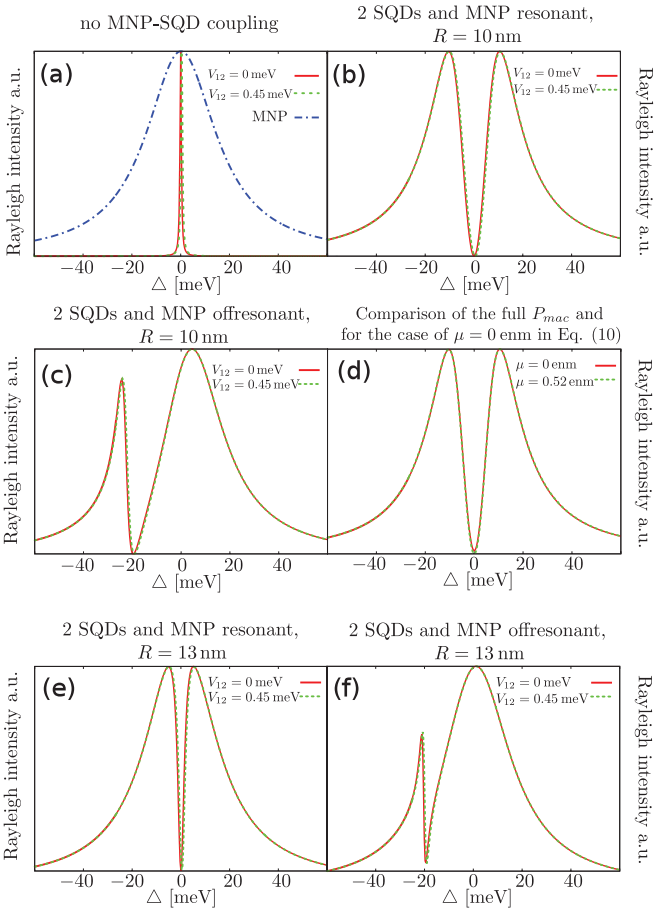

FIG. 3. (Color online) Linear Rayleigh spectra, $I_S = |P(\omega)|^2$, (a) of a MNP and two resonant SQDs without plasmon-SQD interaction, (b) of an MNP and two resonant SQDs in resonance with plasmon-SQD interaction and (c) of an MNP and two resonant SQDs detuned by 19.75 meV with plasmon-SQD interaction. The spectra with solid red lines are calculated without Förster interaction $V_{12} = 0$ meV and the green dashed one with an interaction strength of $V_{12} = 0.45$ meV. (d) compares the Rayleigh spectra of the full macroscopic polarization P_{mac}, Eq. (10), with the polarization operator $P = \chi a + \text{c.c.}$ consisting of the plasmon polarization only. Δ is the detuning of the external optical field and the resonance frequency. In all figures, the SQDs are resonant ($\omega_{g_1} = \omega_{g_2}$). For $R = 10$ nm, the corresponding coupling strength between the plasmons and excitons is $g = 10.96$ meV and $R = 13$ nm corresponds to $g = 4.99$ meV.

the SQD-plasmon coupling. The energy shift δ caused by the Förster interaction V_{12} between the two SQDs in the absence of the MNP is given by[24]

$$\delta = \tfrac{1}{2}\left(\Delta_g \pm \sqrt{\Delta_g^2 + 4V_{12}^2}\right), \tag{17}$$

where Δ_g is the bare detuning between the SQDs. For two resonant SQDs, the formula for the energy shift simplifies to $\delta = \pm V_{12}$.

Comparing the spectra with and without SQD-SQD coupling V_{12}, it is obvious that the Förster interaction V_{12} shifts the transition energies only slightly to higher energies; the coupling between the two resonant SQDs results in the formation of a bright and a dark state, respectively. In the case of two identical SQDs, the dark state is not optically

excitable and therefore not visible in the Rayleigh spectrum [cf. Fig. 3(a)]: only one peak (green dashed) for the SQD resonance is visible. Even the presence of the MNP does not allow to excite the dark state [see Figs. 3(b) and 3(e)]. It is important to note that besides the shift of the transition, caused by the Förster interaction, the spectra in Figs. 3(b), 3(c), 3(e), and 3(f) do not change significantly.

We also compare the linear Rayleigh spectra for the full polarization operator P_{mac}, Eq. (10), with the one occurring from the polarization operator $P = \chi a + \text{c.c.}$ alone, consisting only of the plasmon polarization, where, however, the dynamical equations of the SQDs fully include the $\mu \neq 0$ contribution. We find that the contribution originating from the SQDs in Eq. (10), $\mu_i a^\dagger_{c_i} a_{v_i} + \text{H.c.}$ does not change the Rayleigh spectra significantly, cf. Fig. 3(d), due to the small SQD dipole moment compared to the plasmon dipole moment. In the limit $R \to \infty$, that means without interaction between the SQDs and the MNP, the absorption spectra are simply added. In the next section, we will show that even if the Förster interaction between the SQDs is unimportant for the light scattering spectra, it is of dramatic importance for the emission statistics.

VI. INFLUENCE OF THE FÖRSTER INTERACTION ON THE PLASMON STATISTICS

In this section, we investigate the influence of the Förster interaction (g_i, V_{12}) on the statistics of the plasmons. In particular, we focus on the second-order correlation function $g^{(2)}$, Eq. (12), under stationary excitation: if the $g^{(2)}$ function has a value below 1, the plasmons are antibunched. This is a typical value, e.g., for a single plasmon/photon emitter. For values greater than 1, the plasmons are bunched. An example for such a statistics is a thermal distribution ($g^{(2)} = 2$). The Poisson distribution, typical for coherent radiation, is characterized by a value of $g^{(2)} = 1$.

In particular, we will compare the photon statistics of the hybrid, i.e., the $g^{(2)}$ function for the case where the Förster interaction between the two quantum dots is switched off and on. The two different cases are barely distinguished in the linear Rayleigh spectra, Fig. 3. The most important result of our paper is that in contrast to the Rayleigh spectrum the (nonlinear) plasmon statistics is strongly influenced by the Förster interaction between the SQDs.

To investigate the influence of the Förster interaction on the statistics of the emitted light, we calculate the second-order correlation function (12) for continuous wave excitation in steady state. For this purpose, we solve the coupled equations of motion of the hybrid system numerically until the plasmon density and the plasmon density correlations reached a stationary value, at time t_{stat}. We iterate this calculation for several frequencies of the external optical pump field to obtain Fig. 4. In Fig. 4(a), we plot, for two SQDs and the MNP resonant to each other, the second-order correlation function, Eq. (12), as a function of the excitation frequency of the external optical field with respect to the resonance frequency of the bare MNP (detuning Δ) for three cases; we compare the $g^{(2)}$ function of a hybrid system with and without Förster interaction V_{12}, as well as two different distances between the SQDs and the MNP for weak optical excitation

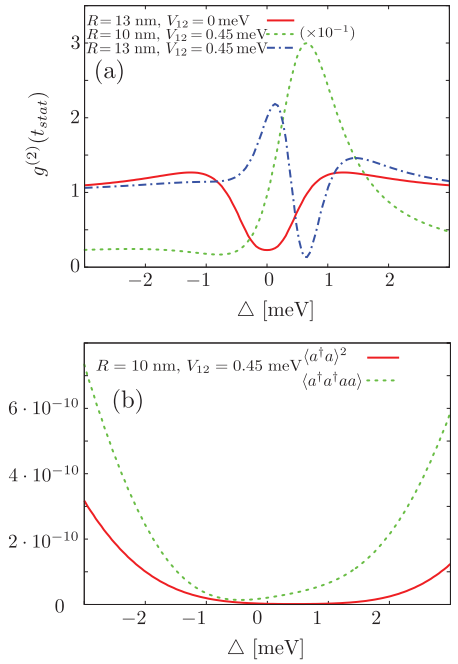

FIG. 4. (Color online) (a) Plot of the stationary $g^{(2)}$ function of the plasmons for two SQDs resonant to each other and to the MNP for a displacement of $R = 10$ nm ($g = 10.96$ meV) between the particles, with and without Förster interaction, and for $R = 13$ nm ($g = 4.99$ meV) with Förster interaction vs the detuning of the resonance frequencies to the external optical field. The curve for $R = 10$ nm and a Förster interaction strength of $V_{12} = 0.45$ meV is divided by 10. (b) Plot of the square of the plasmon density $\langle a^\dagger a\rangle^2$ and of the plasmon correlation $\langle a^\dagger a^\dagger a a\rangle$ for $R = 10$ nm and a Förster interaction strength of $V_{12} = 0.45$ meV vs the detuning ($\Delta = \omega_{\mathrm{sp}} - \omega_{\mathrm{ext}}$) of the resonance frequencies to the external optical field.

($\Omega = 10^{-6}$ eV). The variation in the distance corresponds to a variation of the interaction strength g_i between the ith SQD and the MNP. In contrast to the Rayleigh signal Fig. 3, the different curves in Fig. 4(a) show strong deviations, while varying the Förster interaction strength between the SQDs.

We describe Fig. 4(a) in detail: for all curves, at frequencies far away from the excitonic transition, the second-order correlation function is equal to one, the value of the bare MNP.[17] Near the resonances of the SQDs, however, the $g^{(2)}(t_{\mathrm{stat}})$ function is strongly influenced by the interaction between the MNP and the SQDs. Depending on the frequency of the external field and the distance R, the plasmons can be bunched, antibunched, or coherent. For the case with no Förster interaction between the dots, i.e., $V_{12} = 0$ meV [Fig. 4(a), solid red curve] a symmetric line shape for the $g^{(2)}$ function occurs. A detailed discussion is given below. Including the Förster coupling between the SQDs gives rise of an asymmetric line shape of the $g^{(2)}$ function over the detuning ($\Delta = \omega_{\mathrm{sp}} - \omega_{\mathrm{ext}}$) of the excitation frequency ω_{ext} with respect to the plasma frequency ω_{sp}. For a distance of $R = 10$ nm ($g = 10.96$ meV), we find a huge bunching (corresponding curve divided by 10) of the emitted light near $\Delta = 0.66$ meV. On the other

hand, for a distance of $R = 13$ nm ($g = 4.99$ meV), we find antibunching near $\Delta = 0.66$ meV.

We start with the explanation for the simplest case, without Förster interaction between the SQDs, $V_{12} = 0$ meV, and $R = 13$ nm [solid red, in Fig. 4(a)]. The dipole-dipole interaction between the plasmons in the MNP and excitons in the SQDs forms excited polariton states within the coupled hybrid system (cf. Appendix A). To explain the observed symmetry in Fig. 4(a) (red), we calculate the new eigenenergies of the system by diagonalizing the system matrix. This yields the new eigenenergies of the single excitation contributing to linear optics of the coupled system without Förster interaction V_{12} between the dots: $\hbar\omega_{\rm sp}$ and $\hbar\omega_{\rm sp} \pm \sqrt{2}\hbar g$.[25] Valid in the case of two identical SQDs ($\mu_i = \mu$) with the same coupling strength to the MNP ($g_i = g$) and with the same transition energies of the SQDs and MNP ($\hbar\omega_{g_i} = \hbar\omega_g = \hbar\omega_{\rm sp}$). With this restriction, the dipole moments of the coupled MNP-SQD system for $V_{12} = 0$ meV are given by a combination of the bare dipole moments of the constituents χ and $\mu_i = \mu$ as $0\,e$ nm and $\chi\sqrt{2} \pm \mu$. Since the dipole moment of the plasmons χ is much bigger than the dipole moments of the SQDs μ ($\sqrt{2}\chi \pm \mu \approx \sqrt{2}\chi$) and the eigenenergies of the coupled system are symmetric for $V_{12} = 0$ meV, the second-order correlation function is symmetric too. The antibunching at $\Delta = 0$ meV can be traced back to a reduction of two plasmon events, i.e., the value $\langle|2\rangle\langle 2|\rangle$ with respect to $\langle|1\rangle\langle 1|\rangle$ (c.f. Fig. 5) due to the interaction between the MNP and the SQDs. This reduction of two plasmon events is caused by a superposition and mixing of the newly formed states (c.f. Appendix A) provoked by the interaction g_i between the SQDs and the MNP. Since $\langle|2\rangle\langle 2|\rangle$ is the leading term for the plasmon density correlation $\langle a^\dagger a^\dagger aa\rangle$ (14), the plasmon density correlation is smaller than the square of the plasmon density ($\langle a^\dagger a\rangle^2$), giving rise to antibunching at $\Delta = 0$ meV.

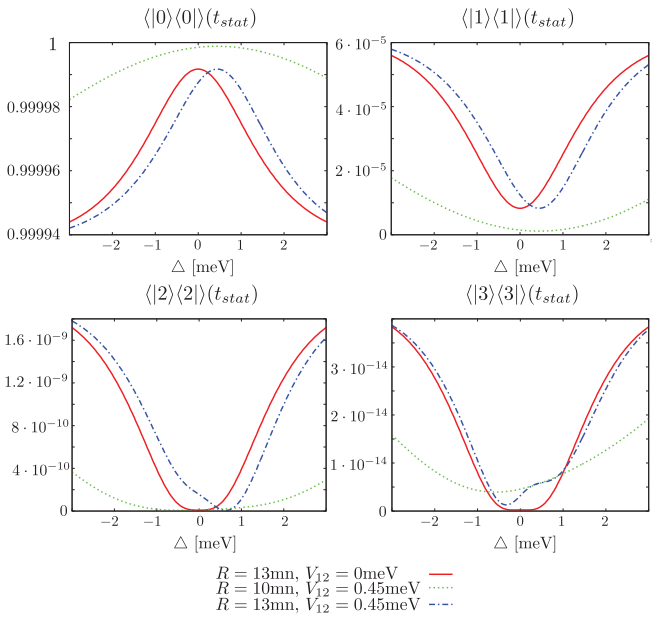

FIG. 5. (Color online) The probability distribution of finding n plasmons ($\langle|n\rangle\langle n|\rangle$) in the system for $n = 0, \ldots, 3$ vs the detuning of the resonances to the external optical field. The curves are for the distances $R = 10$ and 13 nm, respectively, with and without Förster interaction.

Next, the formation of the different light statistics is discussed in detail for the distance $R = 10$ nm with Förster interaction between the dots $V_{12} = 0.45$ meV (green dashed, Fig. 4); here, an asymmetric line shape is observed. Mathematically, the effect is caused by newly occurring different asymmetric distributions in the plasmon density $\langle a^\dagger a\rangle(\omega_{\rm ext})$ and plasmon density correlation $\langle a^\dagger a^\dagger aa\rangle(\omega_{\rm ext})$ [cf. Fig. 4(b)] entering in Eq. (12). This asymmetry is induced by the additional coupling between the SQDs ($V_{12} = 0.45$ meV). Again, we calculate the eigenenergies of the coupled system via the system matrix in the linear regime for identical SQDs ($\mu_i = \mu$), an equal coupling strength between the SQDs to the MNP ($g_i = g$) and resonant transition energies ($\hbar\omega_{g_i} = \hbar\omega_g = \hbar\omega_{\rm sp}$). We find, for the eigenenergies of the single excitations with Förster interaction between the SQDs, the new energies: $\hbar\omega_{\rm sp} - V_{12}$ and $1/2(2\hbar\omega_{\rm sp} + V_{12} \pm \sqrt{8g^2 + V_{12}^2})$. Furthermore, we find the total dipole moments $\mu_{\rm tot}$ of the fully coupled system to be $\mu_{\rm tot} = 0\,e$ nm and

$$\mu_{\rm tot} = \sqrt{2 \pm \frac{2V_{12}}{\sqrt{8g^2 + V_{12}^2}}}\left(\frac{\chi}{2} + \mu\frac{V_{12}}{4g} \mp \mu\sqrt{\frac{1}{2} + \frac{V_{12}^2}{16g^2}}\right). \tag{18}$$

Obviously, the additional Förster coupling between the two SQDs (V_{12}) causes an asymmetry in the eigenenergies and the dipole moments of the coupled system, giving rise to an asymmetric spectrum (c.f. Fig. 6). A detailed discussion of the observed polariton states and its formation due to the Förster interaction V_{12} between the SQDs can be found in the Appendix A. Since $V_{12} \neq 0$ meV redistributes the oscillator strength (dark state lower in energy compared to bright state), we find an enhanced dipole moment for the transitions with a frequency higher than the bare plasmon frequency. Interestingly, the changes in the dipole moments are not only related to the Förster interaction V_{12} between the SQDs but also scale with the interaction strength g between the SQDs and the MNP [c.f. Eq. (18)]. For observables like the plasmon density or the plasmon density correlation, polariton states with higher levels of excitation than the ground-state and single-excitation states enter the calculation. However, the qualitative picture of the asymmetry of the transition energies does not change much compared to the states contributing in linear optics, since the MNP-SQD coupling increases for higher excitation states (c.f. equations of motion, Appendix B). To understand the different asymmetry in the plasmon density and density correlation, we take a closer look at the plasmon probability $\langle|n\rangle\langle n|\rangle$: the higher the plasmon number n in $\langle|n\rangle\langle n|\rangle$, the higher is the perturbation order in the external optical field for driving the contributing states from the ground state. Therefore the asymmetry introduced through the dipole moments enters in a higher order and enhances the asymmetry of the signatures around the plasmon frequency (see Fig. 5). To $\langle a^\dagger a^\dagger aa\rangle$, the plasmon probability $\langle|n\rangle\langle n|\rangle$ enters with $n(n-1)$ beginning with $n = 2$ causing an increasing visibility of the asymmetry around the plasmon frequency. To $\langle a^\dagger a\rangle$, the plasmon probability $\langle|n\rangle\langle n|\rangle$ enters with n, so less pronounced for higher n than to $\langle a^\dagger a^\dagger aa\rangle$, $\langle|1\rangle\langle 1|\rangle$ enters here with almost

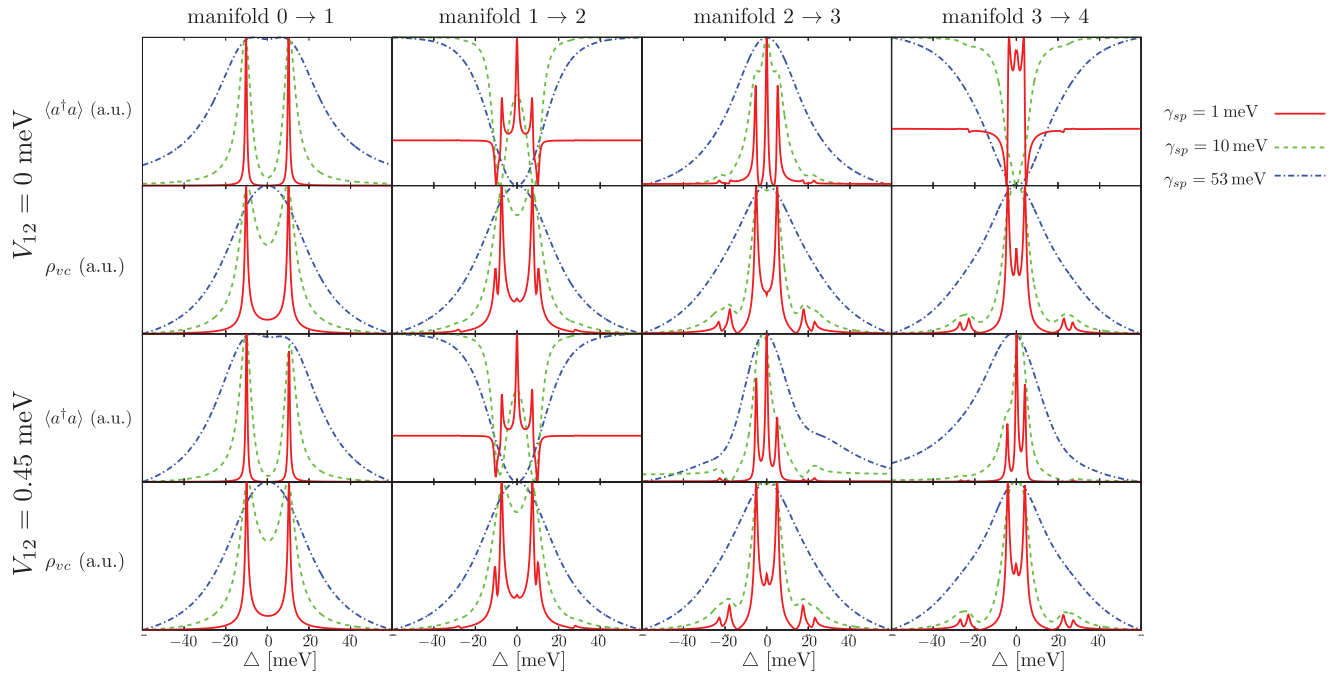

FIG. 6. (Color online) The quantities $\langle a^\dagger a \rangle$ and ρ_{vc} plotted over the detuning ($\Delta = \omega_{\text{sp}} - \omega_{\text{ext}}$) of the resonance frequency of the plasmons with respect to the frequency of the external optical pump field ($\Omega = 10^{-6}$ eV) for a distance $R = 10$ nm, artificially restricting the system to the lowest four transitions from manifold n to $n + 1$, all plots are peak normalized. The upper two rows are without Förster interaction and the lower two rows are with a Förster interaction of $V_{12} = 0.45$ meV for the plasmon density $\langle a^\dagger a \rangle$ and the polarization of the SQD ρ_{vc}, respectively. The solid red curves are for an artificial small damping of the plasmons of $\gamma_{\text{sp}} = 1$ meV, the green dashed one for $\gamma_{\text{sp}} = 10$ meV, and the blue dashed dotted one for a realistic damping of $\gamma_{\text{sp}} = 53.31$ meV.

no asymmetry visible (cf. Fig. 5). Since the $g^{(2)}$ function is the ratio of $\langle a^\dagger a^\dagger a a \rangle$ and $\langle a^\dagger a \rangle^2$, it enhances the visibility of the asymmetry compared to $\langle a^\dagger a \rangle$ and $\langle a^\dagger a^\dagger a a \rangle$ alone. Thus the effects in the $g^{(2)}$ function are the result of a superposition and mixing of the new states formed by the Förster interaction between the excitons and plasmons as well as the Förster interaction between the excitons of the SQDs. These superposition of the newly formed states determines the plasmon density $\langle a^\dagger a \rangle$ as well as the plasmon density correlation $\langle a^\dagger a^\dagger a a \rangle$ and therefore accounts for the observed bunching.

For the distance $R = 13$ nm, the same explanation as for $R = 10$ nm is valid, but it is worth to mention that for $R = 13$ nm the changes in the plasmon polariton states induce a mirrored asymmetry in the plasmon density and density correlation, due to a different coupling strength. This can be seen by inspecting the equivalent to Fig. 6 (not included) for a distance of $R = 13$ nm. Therefore the $g^{(2)}$ function behaves differently and shows antibunching.

The influence of the Förster interaction on the second-order correlation function is investigated in more detail in Fig. 7. Again, we consider two displacements R (10 nm, 13 nm) for a detuning of $\Delta = 0.66$ meV of the external optical field with respect to the resonance frequencies of the particles and resonant excitation $\Delta = 0$ meV. Depending on the displacement R and the coupling strength between the SQDs the statistics of the emitted field shows bunching and antibunching, respectively. Since the $g^{(2)}$ function is given by the ratio of the plasmon density correlation and the square of the plasmon density, it is more sensitive to the symmetry breaking induced by

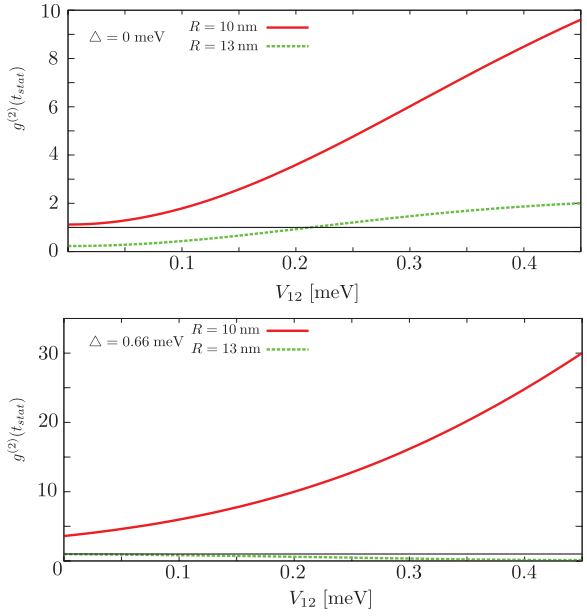

FIG. 7. (Color online) The stationary value of the second-order correlation function for two different distances R and two different detunings Δ of the external pump field and the resonance frequencies are shown. The black solid line indicates the coherent case. For $R = 10$ nm, the corresponding coupling strength between the plasmons and excitons is $g = 10.96$ meV and $R = 13$ nm corresponds to $g = 4.99$ meV.

the Förster interaction between the SQDs than the Rayleigh spectra. Obviously, the Förster interaction is capable to tune the second-order correlation function of the emission over more than one order of magnitude. Even the qualitative character (bunched versus antibunched light) can be influenced in the case of continuous wave excitation.

In both cases, with and without Förster interaction, all effects caused by the SQDs are reduced for increasing displacements R between SQDs and MNP because the coupling strength decreases. The second-order correlation function approaches the behavior of a bare MNP for large distances R. The same effect occurs if the intensity of the external field is increased due to saturation effects of the SQDs.[8] Therefore all calculations are done in the weak-field limit, where no saturation effects of the SQDs take place. An increase or decrease of the pump intensity Ω of around one order of magnitude does not change the $g^{(2)}$ function significantly.

VII. CONCLUSION

Using a fully quantized theory for a hybrid system of a metal nanoparticle and two semiconductor quantum dots, we have shown that the Förster interaction is capable to tune the emission statistics over a wide range from bunched to antibunched light. Experimentally, the interaction between the SQDs can be modified by changing the distance between the SQDs. Depending on the distance between the SQDs and the MNP as well as the Förster interaction strength and light frequency, the hybrid system can behave like a single-photon emitter (antibunching) and a source for chaotic/thermal light (bunching), respectively. Due to these properties, MNP-SQD hybrid systems are of interest for further miniaturization of optical elements on subwavelength scale.

ACKNOWLEDGMENTS

T. S. Theuerholz is grateful for support by the Graduate School of Dynamics in new Light (Leibniz-Gemeinschaft). A. Carmele, M. Richter, and A. Knorr acknowledge support from the Deutsche Forschungsgemeinschaft (SFB 951 HIOS). A.C. gratefully acknowledges also support from the Alexander-von-Humboldt Foundation through the Feodor-Lynen program.

APPENDIX A: PLASMON POLARITON STATES FORMED BY THE INTERACTION BETWEEN THE CONSTITUENTS OF THE HYBRID SYSTEM

The polariton states (formed by MNP and the two SQDs) can be classified using different levels of excitation: each plasmon as well as every individual quantum dot in the excited state counts as one excitation. We discuss the corresponding states for two SQDs and one MNP considering the interaction between the SQDs and with the MNP. The collective states are depicted in Fig. 8. They have one ground state with both SQDs unexcited and no plasmon, the single excitation state of the hybrid system is composed of three states (either one of the SQDs excited or one plasmon in the MNP), and all other states consist of four possible states: n plasmons and both SQDs excited, $n+1$ plasmons and either one SQD excited or $n+3$ plasmons. Between these, manifold transitions from

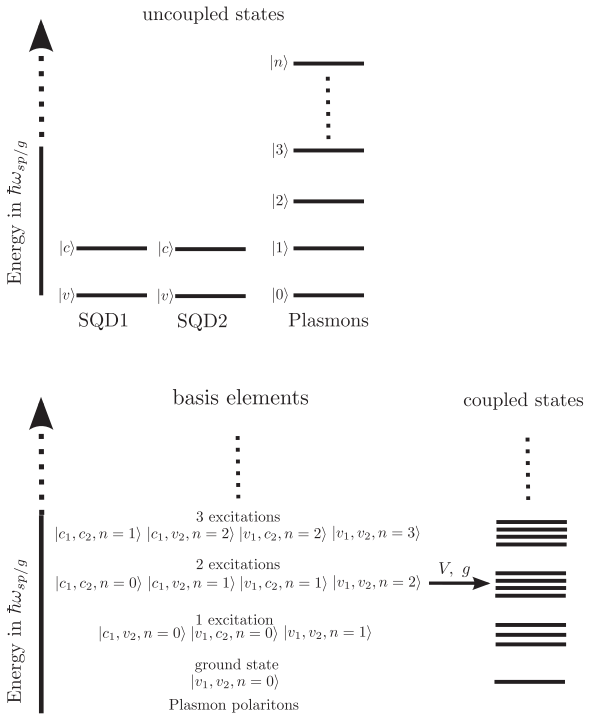

FIG. 8. Sketch of the uncoupled states (top) and of the new quantum states formed by the interaction between the constituents (bottom), for $\hbar\omega_g = \hbar\omega_{\mathrm{sp}}$.

one state to another may occur. So far, these states are the proper energy eigenstates without plasmon-exciton coupling and Förster interaction (cf. basis elements in Fig. 8).

The interaction between the MNP and the SQDs forms new delocalized eigenstates inside the manifolds. These eigenstates are polariton states and determine the dynamics of all our observables. The manifolds correspond, in principle, to an analogon of the Jaynes-Cummings ladder with multiple states on each step of the ladder (cf. coupled states in Fig. 8). In principle, the eigenstates and dipole moments can be calculated by matrix diagonalization. In order to visualize their energies and oscillator strength, we evaluate the dynamics of the observables using a Hilbert space restricted to one excitation manifolds and the next higher one. In this way, we recognize the allowed transition from one manifold to another, cf. Fig. 6. However, due to the large damping of the plasmons (blue dashed dotted) the resonances of the transitions are smeared out. Therefore we also calculated the quantities ($\langle a^\dagger a\rangle$, ρ_{vc}) with an artificial small damping of $\gamma_{\mathrm{sp}} = 1$ meV (red solid) and $\gamma_{\mathrm{sp}} = 10$ meV (green dashed) to clearly observe the energetic structure. For this small damping, the resonances of the transitions between one manifold to another are clearly visible in the spectra. It is worth to mention that some resonances are degenerate and some are dipole forbidden and do not contribute to the optical induced dynamics.

To understand the influence of the damping γ_{sp} on the quantities, we take a closer look at the plasmon density for the transition between manifolds 1 and 2 without Förster interaction in Fig. 6. While the plots with a damping of $\gamma_{\mathrm{sp}} = 1$ meV have five pronounced peaks (at ± 10.2, ± 7.4, and 0 meV), the plots with $\gamma_{\mathrm{sp}} = 10$ meV show only three pronounced peaks. In this case, the peak at ± 7.4 meV seems to decrease.

In fact, a plasmonic transition is dominating this transition, which is highly broadened by the higher damping than the predominating excitonic transitions at ± 10.2 meV. For a realistic plasmon damping, only one peak is visible in the spectra, as a composition of the spectrally wide broadened peaks of the transitions between manifolds 1 and 2.

While the spectra are almost symmetric for the case without Förster interaction between the SQDs in the hybrid structure, they become highly asymmetric if the Förster interaction between the SQDs is taken into account, since the interaction changes the eigenenergies and dipole moments in the excitation manifolds in a very distinct way. This is caused by the additional SQD-SQD interaction, which enhances the nonsymmetric distribution of dipole moments and resonance frequencies. Therefore we cannot anymore classify the energy eigenstates in purely symmetric and antisymmetric states. Interestingly, the spectra of the plasmon density $\langle a^\dagger a\rangle$ are more affected by the Förster interaction than the spectra of the polarization ρ_{vc} of the SQDs, which only become slightly asymmetric. This is caused by the evolution into the steady state: the polarization is created by at least one interaction with the external optical field. The plasmon density is at least created by two subsequent interactions with the external optical field. So the plasmon density is influenced in a higher order by the asymmetry in the dipole moments.

Now, we are going back to the actual dephasing/spectral broadening of the real system without the restriction on certain manifolds and analyze the quantity contribution to the $g^{(2)}$ function, namely, the probability distribution $\langle|n\rangle\langle n|\rangle$ of finding n plasmons in the system (cf. Fig. 5). The position of the resonances and nonsymmetric factors in the probability distributions can be traced back to the shifts and nonsymmetric factors in the manifolds (cf. Fig. 6) and are related to the new formed plasmon polariton exciton states caused by the interaction. Since the probability $\langle|1\rangle\langle 1|\rangle$ has the highest numerical value of all probabilities $\langle|n\rangle\langle n|\rangle (n \geqslant 1)$, in the case of a weak external optical field ($\Omega = 10^{-6}$ eV), it is the leading term for the plasmon density $\langle a^\dagger a\rangle$ [cf. Eq. (12)], therefore this probability will mainly determine the spectral shape of the plasmon density. In contrast to the density, the leading term for the plasmon density correlation $\langle a^\dagger a^\dagger aa\rangle$ is the probability $\langle|2\rangle\langle 2|\rangle$, which will mostly determine the spectral shape of the density correlation. Therefore it is important to mention the change in the line shape between the probabilities $\langle|1\rangle\langle 1|\rangle$ and $\langle|2\rangle\langle 2|\rangle$, which is mostly due to the higher order in light field coupling contribution to $\langle|2\rangle\langle 2|\rangle$, making it more sensitive to changes in the dipole moments.

APPENDIX B: EQUATION OF MOTION

For the sake of completeness, we give the equation of motion for the ρ_{ijkl} terms, for the case of two SQDs:

$$\begin{aligned}\partial_t\langle\rho^{n,m}_{vvvv}\rangle &= \left[\mathbb{i}(n-m)\omega_{\rm sp} - \frac{\gamma_{\rm sp}}{2}(n+m)\right]\langle\rho^{n,m}_{vvvv}\rangle + \gamma_{\rm sp}\sqrt{n+1}\sqrt{m+1}\langle\rho^{n+1,m+1}_{vvvv}\rangle \\ &+ \gamma_g\left(\langle\rho^{n,m}_{cvvc}\rangle + \langle\rho^{n,m}_{vccv}\rangle\right) + \mathbb{i}\frac{\mu_1}{\hbar}\left(E_t^*\langle\rho^{n,m}_{vvvc}\rangle - E_t\langle\rho^{m,n}_{vvvc}\rangle^*\right) + \mathbb{i}\frac{\mu_2}{\hbar}\left(E_t^*\langle\rho^{n,m}_{vvcv}\rangle - E_t\langle\rho^{m,n}_{vvcv}\rangle^*\right) \\ &+ \frac{\mathbb{i}}{\hbar}E_t^*\chi^*\left(\sqrt{m+1}\langle\rho^{n,m+1}_{vvvv}\rangle - \sqrt{n}\langle\rho^{n-1,m}_{vvvv}\rangle\right) + \frac{\mathbb{i}}{\hbar}E_t\chi\left(\sqrt{m}\langle\rho^{n,m-1}_{vvvv}\rangle - \sqrt{n+1}\langle\rho^{n+1,m}_{vvvv}\rangle\right) \\ &+ \mathbb{i}\sqrt{m}g_1\langle\rho^{n,m-1}_{vvvc}\rangle - \mathbb{i}\sqrt{n}g_1^*\langle\rho^{m,n-1}_{vvvc}\rangle^* + \mathbb{i}\sqrt{m}g_2\langle\rho^{n,m-1}_{vvcv}\rangle - \mathbb{i}\sqrt{n}g_2^*\langle\rho^{m,n-1}_{vvcv}\rangle^*. \end{aligned} \tag{B1}$$

The density-like term $\langle\rho^{n,m}_{vvvv}\rangle$ representing the electron ground-state correlation has no decay term but is driven by inscattering terms from upper excitonic levels through $\langle\rho^{n,m}_{cvvc}\rangle$ and $\langle\rho^{n,m}_{vccv}\rangle$. The interaction between the plasmons and the external optical field couples $\langle\rho^{n,m}_{vvvv}\rangle$ to other plasmon number states. The plasmon ecxitation and absorption terms appear at all quantities $\rho^{n,m}_{opqr}$ with $o,p,q,r \in c,v$ (c: conduction, v: valence band).

$$\begin{aligned}\partial_t\langle\rho^{n,m}_{cvcv}\rangle &= \left[\mathbb{i}(n-m)\omega_{\rm sp} + \mathbb{i}\left(\omega_{g_1} - \omega_{g_2}\right) - \frac{\gamma_{\rm sp}}{2}(n+m) - \gamma_g\right]\langle\rho^{n,m}_{cvcv}\rangle + \gamma_{\rm sp}\sqrt{n+1}\sqrt{m+1}\langle\rho^{n+1,m+1}_{cvcv}\rangle \\ &- \mathbb{i}\frac{\mu_1}{\hbar}E_t^*\left(\langle\rho^{n,m}_{vvcv}\rangle - \langle\rho^{m,n}_{ccvc}\rangle^*\right) - \mathbb{i}\frac{\mu_2}{\hbar}E_t\left(\langle\rho^{n,m}_{cccv}\rangle - \langle\rho^{m,n}_{vvvc}\rangle^*\right) + \mathbb{i}\frac{V_{12}}{\hbar}\left(\langle\rho^{n,m}_{vccv}\rangle - \langle\rho^{n,m}_{cvvc}\rangle\right) \\ &+ \frac{\mathbb{i}}{\hbar}E_t^*\chi^*\left(\sqrt{m+1}\langle\rho^{n,m+1}_{cvcv}\rangle - \sqrt{n}\langle\rho^{n-1,m}_{cvcv}\rangle\right) + \frac{\mathbb{i}}{\hbar}E_t\chi\left(\sqrt{m}\langle\rho^{n,m-1}_{cvcv}\rangle - \sqrt{n+1}\langle\rho^{n+1,m}_{cvcv}\rangle\right) \\ &+ \mathbb{i}g_1\sqrt{m}\langle\rho^{m-1,n}_{ccvc}\rangle^* - \mathbb{i}g_1\sqrt{n+1}\langle\rho^{n+1,m}_{vvcv}\rangle + \mathbb{i}g_2^*\sqrt{m+1}\langle\rho^{m+1,n}_{vvvc}\rangle^* - \mathbb{i}g_2^*\sqrt{n}\langle\rho^{n-1,m}_{cccv}\rangle. \end{aligned} \tag{B2}$$

$\langle\rho^{n,m}_{cvcv}\rangle$ is a pure polarization operator for SQD 1 and SQD 2 and therefore damped by γ_g ($\gamma_g/2$ for each transition). The Förster interaction couples $\langle\rho^{n,m}_{cvcv}\rangle$ to pure density like expectation values $\langle\rho^{n,m}_{vccv}\rangle$ and $\langle\rho^{n,m}_{cvvc}\rangle$.

$$\begin{aligned}\partial_t\langle\rho^{n,m}_{cccv}\rangle &= \left[\mathbb{i}(n-m)\omega_{\rm sp} + \mathbb{i}\omega_{g_1} - \frac{\gamma_{\rm sp}}{2}(n+m) - 3/2\gamma_g\right]\langle\rho^{n,m}_{cccv}\rangle + \gamma_{\rm sp}\sqrt{n+1}\sqrt{m+1}\langle\rho^{n+1,m+1}_{cccv}\rangle - \mathbb{i}\frac{\mu_1}{\hbar}E_t^*\left(\langle\rho^{n,m}_{vccv}\rangle - \langle\rho^{n,m}_{cccc}\rangle\right) \\ &- \mathbb{i}\frac{\mu_2}{\hbar}\left(-E_t\langle\rho^{n,m}_{ccvv}\rangle + E_t^*\langle\rho^{n,m}_{cvcv}\rangle\right) - \mathbb{i}\frac{V_{12}}{\hbar}\langle\rho^{n,m}_{cccv}\rangle + \frac{\mathbb{i}}{\hbar}E_t^*\chi^*\left(\sqrt{m+1}\langle\rho^{n,m+1}_{cccv}\rangle - \sqrt{n}\langle\rho^{n-1,m}_{cccv}\rangle\right) + \frac{\mathbb{i}}{\hbar}E_t\chi\left(\sqrt{m}\langle\rho^{n,m-1}_{cccv}\rangle\right. \\ &\left. - \sqrt{n+1}\langle\rho^{n+1,m}_{cccv}\rangle\right) - \mathbb{i}g_1\sqrt{n+1}\langle\rho^{n+1,m}_{vccv}\rangle + \mathbb{i}g_1\sqrt{m}\langle\rho^{n,m-1}_{cccc}\rangle - \mathbb{i}g_2\sqrt{n+1}\langle\rho^{n+1,m}_{cvcv}\rangle + \mathbb{i}g_2^*\sqrt{m+1}\langle\rho^{n,m+1}_{ccvv}\rangle. \end{aligned} \tag{B3}$$

$\langle\rho^{n,m}_{cccv}\rangle$ is a mixed operator, density like for SQD 2 and polarization like for SQD 1 and therefore damped by $3/2\gamma_g$ ($\gamma_g/2$ for the transition and γ_g for the density). Via the conduction band density-like contribution in $\langle\rho^{n,m}_{cccv}\rangle$ it drives the valence band density term in $\langle\rho^{n,m}_{vvvc}\rangle$ [cf. Eq. (B5)]. The Förster interaction couples the density-like part of $\langle\rho^{n,m}_{cccv}\rangle$ to a polarization-like part and vice versa the polarization-like part to a density-like part, this contributes to the formation of plasmon polariton excitations.

$$\begin{aligned}\partial_t\langle\rho^{n,m}_{ccvc}\rangle = &\left[\mathbb{i}(n-m)\omega_{\rm sp}+\mathbb{i}\omega_{g_2}-\frac{\gamma_{\rm sp}}{2}(n+m)-3/2\gamma_g\right]\langle\rho^{n,m}_{ccvc}\rangle+\gamma_{\rm sp}\sqrt{n+1}\sqrt{m+1}\langle\rho^{n+1,m+1}_{ccvc}\rangle\\&-\mathbb{i}\frac{\mu_1}{\hbar}\left(E_t^*\langle\rho^{m,n}_{cvcv}\rangle^*-E_t\langle\rho^{n,m}_{ccvv}\rangle\right)-\mathbb{i}\frac{\mu_2}{\hbar}E_t^*\left(\langle\rho^{n,m}_{cvvc}\rangle-\langle\rho^{n,m}_{cccc}\rangle\right)-\mathbb{i}\frac{V_{12}}{\hbar}\langle\rho^{n,m}_{cccv}\rangle\\&+\frac{\mathbb{i}}{\hbar}E_t^*\chi^*\left(\sqrt{m+1}\langle\rho^{n,m+1}_{ccvc}\rangle-\sqrt{n}\langle\rho^{n-1,m}_{ccvc}\rangle\right)+\frac{\mathbb{i}}{\hbar}E_t\chi\left(\sqrt{m}\langle\rho^{n,m-1}_{ccvc}\rangle-\sqrt{n+1}\langle\rho^{n+1,m}_{ccvc}\rangle\right)\\&-\mathbb{i}\sqrt{n+1}\left(g_1\langle\rho^{m,n+1}_{cvcv}\rangle^*+g_2\langle\rho^{n+1,m}_{cvvc}\rangle\right)+\mathbb{i}g_1^*\sqrt{m+1}\langle\rho^{n,m+1}_{ccvv}\rangle+\mathbb{i}g_2\sqrt{m}\langle\rho^{n,m-1}_{cccc}\rangle.\end{aligned}\tag{B4}$$

$\langle\rho^{n,m}_{ccvc}\rangle$ is, similar to the last term, but in contrast to $\langle\rho^{n,m}_{cccv}\rangle$, the contributions of SQD 1 and SQD 2 are swapped. The Förster interaction couples $\langle\rho^{n,m}_{ccvc}\rangle$ and $\langle\rho^{n,m}_{vvvc}\rangle$.

$$\begin{aligned}\partial_t\langle\rho^{n,m}_{vvvc}\rangle = &\left[\mathbb{i}(n-m)\omega_{\rm sp}-\mathbb{i}\omega_{g_1}-\frac{\gamma_{\rm sp}}{2}(n+m)-1/2\gamma_g\right]\langle\rho^{n,m}_{vvvc}\rangle+\gamma_{\rm sp}\sqrt{n+1}\sqrt{m+1}\langle\rho^{n+1,m+1}_{vvvc}\rangle\\&+\gamma_g\langle\rho^{m,n}_{cccv}\rangle^*-\mathbb{i}\frac{\mu_1}{\hbar}E_t\left(\langle\rho^{n,m}_{cvvc}\rangle-\langle\rho^{n,m}_{vvvv}\rangle\right)+\mathbb{i}\frac{\mu_2}{\hbar}\left(E_t^*\langle\rho^{m,n}_{ccvv}\rangle^*-E_t\langle\rho^{n,m}_{cvcv}\rangle^*\right)-\mathbb{i}\frac{V_{12}}{\hbar}\langle\rho^{n,m}_{vvcv}\rangle\\&+\frac{\mathbb{i}}{\hbar}E_t^*\chi^*\left(\sqrt{m+1}\langle\rho^{n,m+1}_{vvvc}\rangle-\sqrt{n}\langle\rho^{n-1,m}_{vvvc}\rangle\right)+\frac{\mathbb{i}}{\hbar}E_t\chi\left(\sqrt{m}\langle\rho^{n,m-1}_{vvvc}\rangle-\sqrt{n+1}\langle\rho^{n+1,m}_{vvvc}\rangle\right)\\&+\mathbb{i}g_2\sqrt{m}\langle\rho^{m-1,n}_{ccvv}\rangle^*-\mathbb{i}g_2^*\sqrt{n}\langle\rho^{m,n-1}_{cvcv}\rangle^*+\mathbb{i}g_1^*\sqrt{m+1}\langle\rho^{n,m+1}_{vvvv}\rangle-\mathbb{i}g_1^*\sqrt{n}\langle\rho^{n-1,m}_{cvvc}\rangle.\end{aligned}\tag{B5}$$

Similar to the last to terms $\langle\rho^{n,m}_{vvcv}\rangle$ is a mixed operator, but now the density-like part belongs to the valence band. This affects the damping and gives rise of the driving term $\langle\rho^{n,m}_{cccv}\rangle$ in the second line. Again, the Förster interaction couples the density-like part to a polarization-like part and the polarization part to a density part.

$$\begin{aligned}\partial_t\langle\rho^{n,m}_{vvcv}\rangle = &\left[\mathbb{i}(n-m)\omega_{\rm sp}-\mathbb{i}\omega_{g_2}-\frac{\gamma_{\rm sp}}{2}(n+m)-1/2\gamma_g\right]\langle\rho^{n,m}_{vvcv}\rangle+\gamma_{\rm sp}\sqrt{n+1}\sqrt{m+1}\langle\rho^{n+1,m+1}_{vvcv}\rangle\\&+\mathbb{i}\frac{\mu_1}{\hbar}\left(E_t^*\langle\rho^{m,n}_{ccvv}\rangle^*-E_t\langle\rho^{n,m}_{cvcv}\rangle\right)+\mathbb{i}\frac{\mu_2}{\hbar}E_t\left(\langle\rho^{n,m}_{vvvv}\rangle-\langle\rho^{n,m}_{vccv}\rangle\right)-\mathbb{i}\frac{V_{12}}{\hbar}\langle\rho^{n,m}_{vvvc}\rangle+\gamma_g\langle\rho^{m,n}_{ccvc}\rangle^*\\&+\frac{\mathbb{i}}{\hbar}E_t^*\chi^*\left(\sqrt{m+1}\langle\rho^{n,m+1}_{vvcv}\rangle-\sqrt{n}\langle\rho^{n-1,m}_{vvcv}\rangle\right)+\frac{\mathbb{i}}{\hbar}E_t\chi\left(\sqrt{m}\langle\rho^{n,m-1}_{vvcv}\rangle-\sqrt{n+1}\langle\rho^{n+1,m}_{vvcv}\rangle\right)\\&+\mathbb{i}g_1\sqrt{m}\langle\rho^{m-1,n}_{ccvv}\rangle^*-\mathbb{i}g_1^*\sqrt{n}\langle\rho^{n-1,m}_{cvcv}\rangle+\mathbb{i}g_2^*\sqrt{m+1}\langle\rho^{n,m+1}_{vvvv}\rangle-\mathbb{i}g_2^*\sqrt{n}\langle\rho^{n-1,m}_{vccv}\rangle.\end{aligned}\tag{B6}$$

$\langle\rho^{n,m}_{vvcv}\rangle$ behaves like the last term $\langle\rho^{n,m}_{vvvc}\rangle$ with swapped SQDs. Therefore again the Förster interaction couples both terms leading to the new plasmon polariton excitations.

$$\begin{aligned}\partial_t\langle\rho^{n,m}_{ccvv}\rangle = &\left[\mathbb{i}(n-m)\omega_{\rm sp}+\mathbb{i}(\omega_{g_1}+\omega_{g_2})-\frac{\gamma_{\rm sp}}{2}(n+m)-\gamma_g\right]\langle\rho^{n,m}_{ccvv}\rangle+\gamma_{\rm sp}\sqrt{n+1}\sqrt{m+1}\langle\rho^{n+1,m+1}_{ccvv}\rangle\\&-\mathbb{i}\frac{\mu_1}{\hbar}E_t^*\left(\langle\rho^{m,n}_{vvcv}\rangle^*-\langle\rho^{n,m}_{ccvc}\rangle\right)-\mathbb{i}\frac{\mu_2}{\hbar}E_t^*\left(\langle\rho^{m,n}_{vvvc}\rangle^*-\langle\rho^{n,m}_{cccv}\rangle\right)\\&+\frac{\mathbb{i}}{\hbar}E_t^*\chi^*\left(\sqrt{m+1}\langle\rho^{n,m+1}_{ccvv}\rangle-\sqrt{n}\langle\rho^{n-1,m}_{ccvv}\rangle\right)+\frac{\mathbb{i}}{\hbar}E_t\chi\left(\sqrt{m}\langle\rho^{n,m-1}_{ccvv}\rangle-\sqrt{n+1}\langle\rho^{n+1,m}_{ccvv}\rangle\right)\\&+\mathbb{i}g_2\sqrt{m}\langle\rho^{n,m-1}_{cccv}\rangle-\mathbb{i}g_2\sqrt{n+1}\langle\rho^{m,n+1}_{vvvc}\rangle^*+\mathbb{i}g_1\sqrt{m}\langle\rho^{n,m-1}_{ccvc}\rangle-\mathbb{i}g_1\sqrt{n+1}\langle\rho^{m,n+1}_{vvcv}\rangle^*.\end{aligned}\tag{B7}$$

The pure polarization-like term $\langle\rho^{n,m}_{ccvv}\rangle$ is damped by γ_g since it involves the polarization of two SQDs and does not couple via the Förster interaction, since all SQDs are simultaneously either excited or unexcited.

$$\begin{aligned}\partial_t\langle\rho^{n,m}_{vccv}\rangle = &\left[\mathbb{i}(n-m)\omega_{\rm sp}-\frac{\gamma_{\rm sp}}{2}(n+m)-\gamma_g\right]\langle\rho^{n,m}_{vccv}\rangle+\gamma_{\rm sp}\sqrt{n+1}\sqrt{m+1}\langle\rho^{n+1,m+1}_{vccv}\rangle\\&+\mathbb{i}\frac{V_{12}}{\hbar}\left(\langle\rho^{n,m}_{cvcv}\rangle-\langle\rho^{m,n}_{cvcv}\rangle^*\right)+\gamma_g\langle\rho^{n,m}_{cccc}\rangle\\&+\mathbb{i}\frac{\mu_1}{\hbar}\left(E_t^*\langle\rho^{m,n}_{cccv}\rangle^*-E_t\langle\rho^{n,m}_{cccv}\rangle\right)+\mathbb{i}\frac{\mu_2}{\hbar}\left(E_t\langle\rho^{m,n}_{vvcv}\rangle^*-E_t^*\langle\rho^{n,m}_{vvcv}\rangle\right)\\&+\frac{\mathbb{i}}{\hbar}E_t^*\chi^*\left(\sqrt{m+1}\langle\rho^{n,m+1}_{vccv}\rangle-\sqrt{n}\langle\rho^{n-1,m}_{vccv}\rangle\right)+\frac{\mathbb{i}}{\hbar}E_t\chi\left(\sqrt{m}\langle\rho^{n,m-1}_{vccv}\rangle-\sqrt{n+1}\langle\rho^{n+1,m}_{vccv}\rangle\right)\\&+\mathbb{i}g_1\sqrt{m}\langle\rho^{m-1,n}_{cccv}\rangle^*-\mathbb{i}g_1^*\sqrt{n}\langle\rho^{n-1,m}_{cccv}\rangle+\mathbb{i}g_2^*\sqrt{m+1}\langle\rho^{m+1,n}_{vvcv}\rangle^*-\mathbb{i}g_2\sqrt{n+1}\langle\rho^{n+1,m}_{vvcv}\rangle.\end{aligned}\tag{B8}$$

In the pure density-like term $\langle\rho^{n,m}_{vccv}\rangle$, we can again see the driving of the valance-band-like part through the corresponding conduction band part of $\langle\rho^{n,m}_{cccc}\rangle$. Via the Förster interaction $\langle\rho^{n,m}_{vccv}\rangle$ is coupled to the pure polarization-like term $\langle\rho^{n,m}_{cvcv}\rangle$.

$$\begin{aligned}\partial_t\langle\rho^{n,m}_{cvvc}\rangle = &\left[\mathbb{i}(n-m)\omega_{\mathrm{sp}} - \frac{\gamma_{\mathrm{sp}}}{2}(n+m) - \gamma_g\right]\langle\rho^{n,m}_{cvvc}\rangle + \gamma_{\mathrm{sp}}\sqrt{n+1}\sqrt{m+1}\langle\rho^{n+1,m+1}_{cvvc}\rangle + \mathbb{i}\frac{V_{12}}{\hbar}\left(\langle\rho^{m,n}_{cvcv}\rangle^* - \langle\rho^{n,m}_{cvcv}\rangle\right) + \gamma_g\langle\rho^{n,m}_{cccc}\rangle\\ &+ \mathbb{i}\frac{\mu_1}{\hbar}E_t\langle\rho^{m,n}_{vvvc}\rangle^* - \mathbb{i}\frac{\mu_1}{\hbar}E_t^*\langle\rho^{n,m}_{vvvc}\rangle + \mathbb{i}\frac{\mu_2}{\hbar}E_t^*\langle\rho^{m,n}_{ccvc}\rangle^* - \mathbb{i}\frac{\mu_2}{\hbar}E_t\langle\rho^{n,m}_{ccvc}\rangle + \frac{\mathbb{i}}{\hbar}E_t^*\chi^*\left(\sqrt{m+1}\langle\rho^{n,m+1}_{cvvc}\rangle - \sqrt{n}\langle\rho^{n-1,m}_{cvvc}\rangle\right)\\ &+ \frac{\mathbb{i}}{\hbar}E_t\chi\left(\sqrt{m}\langle\rho^{n,m-1}_{cvvc}\rangle - \sqrt{n+1}\langle\rho^{n+1,m}_{cvvc}\rangle\right) + \mathbb{i}g_1^*\sqrt{m+1}\langle\rho^{m+1,n}_{vvvc}\rangle^* - \mathbb{i}g_1\sqrt{n+1}\langle\rho^{n+1,m}_{vvvc}\rangle\\ &+ \mathbb{i}g_2\sqrt{m}\langle\rho^{m-1,n}_{ccvc}\rangle^* - \mathbb{i}g_2^*\sqrt{n}\langle\rho^{n-1,m}_{ccvc}\rangle. \qquad \text{(B9)}\end{aligned}$$

The term $\langle\rho^{n,m}_{cvvc}\rangle$ behaves in the same way as the last one ($\langle\rho^{n,m}_{vccv}\rangle$) with swapped SQD 1 and SQD 2.

Restricting ourself to two SQDs and assuming only one electron per SQD in Eqs. (B1)–(B9), the hierarchy of the electron operators is closed at the level of expectation values with four operators. With this assumption, higher orders of electron operators do not exist.

*theuerholz@itp.tu-berlin.de

[1] S. Gaponenko and D. Guzatov, Chem. Phys. Lett. **477**, 411 (2009).

[2] Jeffrey N. Anker, W. Paige Hall, Olga Lyandres, Nilam C. Shah, Jing Zhao, and Richard P. Van Duyne, Nat. Mater. **7**, 442 (2008).

[3] Harry A. Atwater and Albert Polman, Nat. Mater. **9**, 205 (2010).

[4] M. Barth, S. Schietinger, T. Schröder, T. Aichele, and O. Benson, J. Lumin. **130**, 1628 (2010).

[5] M. A. Noginov, G. Zhu, A. M. Belgrave, R. Bakker, V. M. Shalaev, E. E. Narimanov, S. Stout, E. Herz, T. Suteewong, and W. Wiesner, Nature (London) **460**, 1110 (2009).

[6] D. J. Bergman and M. I. Stockman, Phys. Rev. Lett. **90**, 027402 (2003).

[7] A. O. Govorov, J. Lee, and N. A. Kotov, Phys. Rev. B **76**, 125308 (2007).

[8] A. Ridolfo, O. Di Stefano, N. Fina, R. Saija, and S. Savasta, Phys. Rev. Lett. **105**, 263601 (2010).

[9] Y. He and K.-D. Zhu, Nanoscale Res. Lett. **7**, 95 (2012).

[10] S. M. Sadeghi, Phys. Rev. B **79**, 233309 (2009).

[11] J.-Y. Yan, W. Zhang, S. Duan, X.-G. Zhao, and A. O. Govorov, Phys. Rev. B **77**, 165301 (2008).

[12] C. Van Vlack, P. T. Kristensen, and S. Hughes, Phys. Rev. B **85**, 075303 (2012).

[13] T. Förster, Discuss. Faraday Soc. **27**, 7 (1959).

[14] M. Richter, K. J. Ahn, A. Knorr, A. Schliwa, D. Bimberg, M. E.-A. Madjet, and T. Renger, Phys. Status Solidi B **243**, 2302 (2006).

[15] A. Sitek and P. Machnikowski, Phys. Status Solidi B **248**, 847 (2011).

[16] M. O. Scully and M. S. Zubairy, *Quantum Optics* (Cambridge University Press, Cambridge, 2001).

[17] E. Waks and D. Sridharan, Phys. Rev. A **82**, 043845 (2010).

[18] B. W. Lovett, J. H. Reina, A. Nazir, and G. A. D. Briggs, Phys. Rev. B **68**, 205319 (2003).

[19] S. A. Crooker, J. A. Hollingsworth, S. Tretiak, and V. I. Klimov, Phys. Rev. Lett. **89**, 186802 (2002).

[20] P. B. Johnson and R. W. Christy, Phys. Rev. B **6**, 4370 (1972).

[21] R. Loudon, *The Quantum Theory of Light*, 3rd ed. (Oxford University Press, New York, 2000).

[22] A. G. Curto, G. Volpe, T. H. Taminiau, M. P. Kreuzer, R. Quidant, and N. F. van Hulst, Science **329**, 930 (2010).

[23] M. Richter, A. Carmele, A. Sitek, and A. Knorr, Phys. Rev. Lett. **103**, 087407 (2009).

[24] J. Danckwerts, K. J. Ahn, J. Förstner, and A. Knorr, Phys. Rev. B **73**, 165318 (2006).

[25] Important for understanding the symmetries is that the MNP to SQD coupling g_i enters twice as coupling between MNP and SQD 1 and between MNP and SQD 2, where the asymmetry of the two occurring from the coupling is computationally itself.